A-priori testing of sub-grid models for chemically reacting nonpremixed turbulent shear flows

By J. Jiménez[1], A. Liñán[2], M. M. Rogers[3] AND F. J. Higuera[2]

The β-assumed-pdf approximation of (Cook & Riley 1994) is tested as a subgrid model for the LES computation of nonpremixed turbulent reacting flows, in the limit of cold infinitely fast chemistry, for two plane turbulent mixing layers with different degrees of intermittency. Excellent results are obtained for the computation of integrals properties such as product mass fraction, and the model is applied to other quantities such as powers of the temperature and the pdf of the scalar itself. Even in these cases the errors are small enough to be useful in practical applications. The analysis is extended to slightly out of equilibrium problems such as the generation of radicals, and formulated in terms of the pdf of the scalar gradients. It is shown that the conditional gradient distribution is universal in a wide range of cases whose limits are established. Within those limits, engineering approximations to the radical concentration are also possible. It is argued that the experiments in this paper are essentially in the limit of infinite Reynolds number.

1. Introduction

The computation of turbulent reacting flows is an open challenge even after having been the focus of intensive work for several decades. The subject of the present note, nonpremixed flames with fast chemistry, was one of the first to be tackled, and it is somewhat simpler than others, but it still represents a large number of cases of theoretical and practical importance. Recent reviews can be found in (Bilger 1989, Libby & Williams 1994).

Our analysis is subject to several simplifications. The diffusion coefficients of all the species and of heat are assumed to be identical, $\kappa_i = \kappa$ and, although not explicitly needed for most of the theoretical arguments, all of our numerical experiments are done at Schmidt number $Sc = 0.7$. Our flows are incompressible, and we assume that any heat released by the reaction is weak enough for the fluid density to be unchanged, $\rho = 1$. The role of the chemistry is thus passive with respect to the flow, although it is modified by it.

In most cases we assume an irreversible binary reaction

$$\nu_A A + \nu_B B \rightarrow \nu_P P, \tag{1}$$

in a shear flow between two streams, each of which initially contains either pure A or B reactant.

1 Center for Turbulence Research
2 School of Aeronautics, U. Politécnica, Madrid
3 NASA Ames Research Center

Under those circumstances the mass fractions Y_i of the different species can be linearly combined to form a set of conserved scalars which are transported by the flow with the common diffusion coefficient κ. If in addition the Damköhler number, which measures the ratio of the characteristic diffusion and chemical times, is large enough, the reaction occurs in a thin flame that can be treated as a surface, and the problem reduces to the mixing of a single conserved scalar

$$\xi = \frac{Y_{A0} - Y_A + rY_B}{Y_{A0} + rY_{B0}}, \tag{2}$$

called the mixture fraction, which takes values $\xi = 0$ and $\xi = 1$ at the free streams (see Williams 1985). Here Y_{i0} is the mass fraction of the i-th species at the appropriate free stream, and

$$r = \nu_A W_A / \nu_B W_B, \tag{3}$$

where ν_i and W_i are stoichiometric coefficients and molecular weights. The flame is located at the stoichiometric mixture fraction

$$\xi_s = \frac{Y_{A0}}{Y_{A0} + rY_{B0}}, \tag{4}$$

and most quantities of interest can be computed as algebraic functions of ξ, which are continuous but have discontinuous derivatives ξ_s. Thus the mass fraction of the product Y_P is proportional to the triangular function

$$f(\xi) = \xi/\xi_s \quad \text{if} \quad \xi \le \xi_s, \qquad (1-\xi)/(1-\xi_s) \quad \text{otherwise.} \tag{5}$$

In modeling turbulent flows we can usually estimate averaged or locally filtered values of ξ, and we would like to have similarly filtered values of mass fractions or other quantities, but we are prevented from doing so by the nonlinear nature of (5).

It was realized soon that what is needed is an approximation to the probability density function (pdf) of ξ, and that the mean value of any quantity which can be expressed as a function of ξ is (Lin & O'Brien 1974, Bilger 1976)

$$\langle f \rangle = \int f(\xi) p(\xi)\, \mathrm{d}\xi, \tag{6}$$

where $p(\xi)$ is the pdf. Numerous experimental (LaRue & Libby 1974, Anselmet & Antonia 1978, Breidenthal 1981, Mungal & Dimotakis 1984, Koochesfahani & Dimotakis 1986), theoretical or numerical (Eswaran & Pope 1988, Pumir 1994, Holzer & Siggia 1994), and modeling (Kollman & Janicka 1982, Broadwell & Breidenthal 1982) efforts have been undertaken to understand the properties of the pdf of passively mixed scalars.

Of particular interest in this report is the β-pdf model of (Cook & Riley 1994), in which the form of the scalar pdf is modeled as a function of its mean value and standard deviation and, especially, its use as a sub-grid model for large eddy simulations (LES). Large eddy simulation has proven to be a powerful technique for

the computation of complex flows and good results have been obtained in the computation of filtered scalar mean values (Lesieur & Rogallo 1989, Moin *et al.* 1991). We will show below that the subgrid fluctuation intensity can also be estimated with good accuracy. In this report we will assume that exact filtered mean scalar values can be computed by some LES scheme, but we will obtain them by filtering direct numerical simulation fields. The β-pdf model has been tested in this way for isotropic turbulent flow at relatively low Reynolds numbers in (Cook & Riley 1994, Réveillon & Vervisch 1996). We will test it here in the more realistic case of a mixing layer at medium Reynolds numbers (Rogers & Moser 1994).

At issue is the question of large-scale turbulent intermittency, which is the presence of essentially laminar pockets in an otherwise turbulent flow, and whether the same subgrid mixing model can be used in homogeneous turbulence and in the presumed interface between turbulent and laminar regions. A lot of effort has gone into modeling such intermittency effects (Libby 1975, Dopazo 1977, Kollman 1984, Pope 1985, Pope & Correa 1988) but, if it is really a large scale effect, LES should be able to resolve it without resorting to modeling. The main difference between homogeneous flows and the mixing layer is that, while large-scale intermittency is rare in the former, it is prevalent in the latter.

The simulation experiments are described in the next section. The results of applying the β-pdf model to the prediction of different quantities in infinitely fast chemistry are presented in §3. We then extend the model to finite rate chemistry in the flamelet limit, and introduce some results on the joint pdf of the scalar and the scalar gradients, followed by discussion and conclusions.

2. Numerical experiments

The two flow fields used in this report are taken from the simulations in (Rogers & Moser 1994), where they are described in detail. Briefly, they are direct simulations of three-dimensional, temporally growing mixing layers, spatially periodic in the streamwise and spanwise directions, with initial conditions which represent turbulent boundary layers. The flow fields chosen are those in Figs. 18.a and 18.c of that paper, at which time the momentum thickness, θ, of the layers has grown by factors of 2.47 and 2.94 respectively from the initial conditions, and the streamwise integral scale has increased by a factor of about four. The energy spectra have a short power-law range with an exponent close to $-5/3$, and the layers are growing self-similarly. Both layers appear to be slightly beyond the "mixing transition" identified in (Konrad 1976, Breidenthal 1981). The Reynolds numbers based on the instantaneous momentum thickness are 1980 and 2350, and correspond to longitudinal microscale Reynolds numbers $Re_\lambda = 127$ and 214 at the central plane of the layer. Note that both flows are quite intermittent, especially the second one, and that these values would probably change if they were conditioned only to the turbulent fluid. The ratio between vorticity and momentum thickness is about 4.85 in both cases.

The computational boxes are, in both cases, 125×31.25 initial momentum thickness and contain five or six large spanwise structures at the times chosen for our

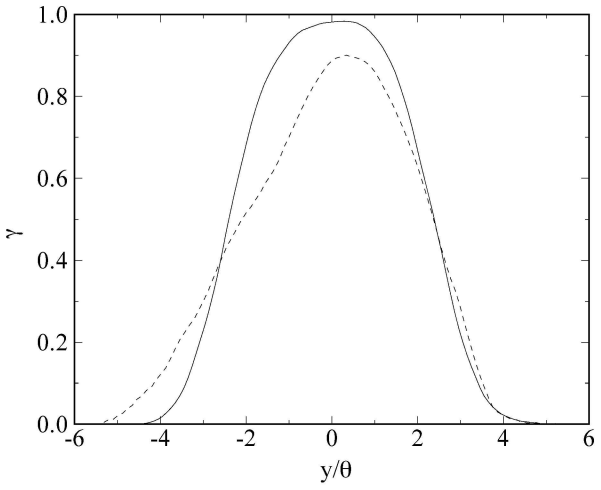

FIGURE 1. Scalar intermittency across the two mixing layers used in the text, defined as the fraction of fluid for which $\xi \in (0.02, 0.98)$. ——— : unforced case. ---- : forced.

experiments. A passive scalar is introduced at the initial condition with a laminar profile of thickness similar to that of the vorticity layer and a range $\xi \in (0, 1)$. Although the original simulations were spectral, using a mesh that was neither uniform nor isotropic, they were spectrally interpolated to physical variables on a uniform isotropic mesh for the purpose of our experiments. This implies some reduction in the resolution, which is dictated by the least resolved direction. Thus while the original computations were carried using $512 \times 180 \times 128$ and $384 \times 96 \times 96$ spectral modes, the interpolated fields contain $512 \times 128 \times 128$ and $384 \times 120 \times 128$ points. The pitch of the interpolated grids is $\Delta x/\theta \approx 0.1$ in both cases, although the original grids are finer by about a factor of two, especially at the central plane and in the transverse, y, direction. All lengths in this report are normalized with the instantaneous momentum thickness of the layers. In terms of the Kolmogorov scale at the center of the layer, $\theta/\eta = 67$ and 72 respectively, and the resolution of our interpolated grid is about 7η in both cases.

It was found in (Rogers & Moser 1994) that the structure of the layer depends during the whole simulation on the initial conditions, corresponding to similar long term effects during the initial development of experimental layers. Different amounts of initial perturbations were introduced in the simulations to mimic this effect. Our two flow fields correspond to two extreme cases in the amount of two-dimensional perturbations applied to the initial conditions. In the first one, which will be referred from now on as the "unforced" case, the initial conditions were synthesized from two turbulent boundary layers without modification. At the time of our experiment, both the vorticity and the scalar field are fairly disorganised with weak spanwise coherent structures, and there is very little fresh fluid at the center of the layer. In contrast, the second case was initialized by amplifying the spanwise-coherent modes of the initial boundary layers by a factor of 20, and the resulting

two-dimensional forcing gives rise to clear spanwise rollers with fresh fluid from one or the other stream present across the layer. This is clear in Fig. 1, which presents the fraction of mixed fluid in both cases, arbitrarily defined as $\xi \in (0.02, 0.98)$. Not only is the mixed fraction higher in the unforced case, but the presence of a few larger structures in the forced one results in insufficient statistics which are not symmetric with respect to the central plane. The statistics for the unforced case are symmetric.

Of the two cases, the forced one is the hardest to compute because of the larger intermittency. Most of the results given below are for this case. The corresponding ones for the unforced case are at least as good, and usually better.

We will generally compare mean quantities, denoted by $\langle\cdot\rangle$, which are averaged over whole $x - z$ planes. Occasionally the averages will be extended to slabs of the mixing layer, in which case the limits of the transverse coordinate y will be given explicitly. In our simulations of LES we define our basic filtering operation as a box filter in physical space. Quantities are averaged over a cubical box of contiguous grid points of side $h = n\Delta x$, and assigned to the center of the box. This operation will be denoted by an overbar. Other filtering kernels have been used by other investigators, and it is not clear which is the best choice to mimic the projection operation implicit in a discrete grid, but our choice seems natural for finite differences or finite volumes codes, and has the advantage of providing a simple definition for subgrid statistics.

Equation (6) extends trivially to filtered quantities, but the pdf has then to be taken to refer only to the interior of the filter box. Thus for a filter of width h we can define a subgrid mean

$$\overline{\xi}(\mathbf{x}) = h^{-3} \int_{h^3} \xi(\mathbf{x} - \mathbf{x}')\, \mathrm{d}^3\mathbf{x}' = \int \xi\, p_h(\xi;\, \mathbf{x})\, \mathrm{d}\xi, \tag{7}$$

and a variance as

$$\xi_h'^2 = \overline{\xi^2} - \overline{\xi}^2. \tag{8}$$

All quantities are functions of y and, in addition, filtered quantities are also functions of the homogeneous coordinates x and z. To increase the number of data points available for the statistics, filtered quantities are computed at all grid points, even if they are only strictly independent over a coarser grid of pitch h. Plane averages are then computed for these filtered quantities and used to generate filtered profiles, which satisfy

$$\langle\overline{f}\rangle = h^{-1} \int_{-h/2}^{h/2} \langle f\rangle\, \mathrm{d}y = \overline{\langle f\rangle}. \tag{9}$$

Note that we can combine (6) and (9) to generate a "filtered" pdf for ξ,

$$\overline{p}(\xi,\, y) = h^{-1} \int_{h/2}^{h/2} p(\xi, y - y')\, \mathrm{d}y', \tag{10}$$

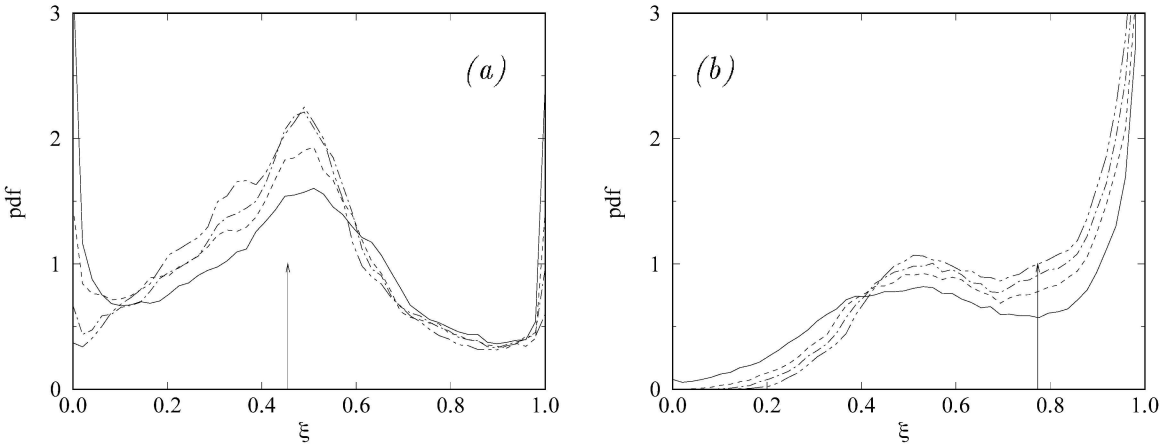

FIGURE 2. Mixture fraction pdfs from LES without subgrid modeling. Forced layer. (a) $y/\theta = 0$. (b) $y/\theta = 3$. ——— : no filter. - - - - : $h/\theta = 0.44$. —·— : 0.66. —··— : 0.88. Vertical arrows mark the mean value of ξ for each plane.

such that (6) generalizes to

$$\overline{\langle f \rangle} = \int f(\xi)\overline{p}(\xi)\,\mathrm{d}\xi. \tag{11}$$

The error of any approximation to the mean profiles depends on our success in approximating $\overline{p}$ from our local models for p_h. In most of our experiments the filter width will be small enough with respect to the width of the layer that we will be able to neglect the difference between laterally filtered and unfiltered pdfs.

3. Fast chemistry

3.1 No subgrid model

It should be clear from the discussion in the last section that the aim of any approximation should be to reproduce $\overline{p}(\xi)$ as closely as possible. In RANS computations, all the available information is the mean value of the mixture fraction over a plane and perhaps some of its statistical moments. Unless some model is applied for the form of the pdf, the implied representation is a delta function $\overline{p} = \delta(\xi - \langle\xi\rangle)$, and is known to be poor.

In LES we have some hope of avoiding subgrid modeling, since the grid elements are small parts of the flow in which the fluid may be assumed to be mixed and well represented by its mean. Large intermittent unmixed regions are hopefully contained in individual grid elements. In this approximation

$$p_h(\xi) = \delta(\xi - \overline{\xi}), \qquad \overline{f(\xi)} = f(\overline{\xi}). \tag{12}$$

In practice the filtered grid values are treated like real points and used to compile statistics.

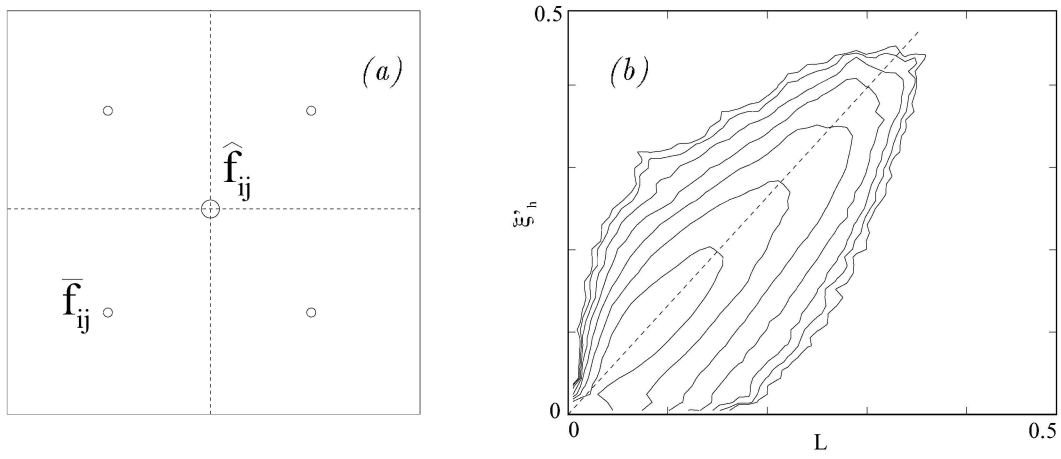

FIGURE 3. (a) Sketch of the two filters for the estimation of the subgrid variance. (b) Joint pdf of the band-passed mixture fraction fluctuation L and its true subgrid value ξ_h'. The dashed line is (15) with spectral slope $-5/3$. Isolines are logarithmically spaced by half an order of magnitude. Forced layer. $y/\theta = (-2,\, 2)$.

The approximation (12) is tested directly in Fig. 2 for the pdfs of the mixture fraction in two planes of the forced mixing layer. Each figure contains the pdfs resulting from several different filters, compared to the real one. The widths of the filters are of the order of the momentum thickness (30-50 Kolmogorov lengths), and correspond to grids of 10-20 points across the layer (Fig. 1). Even with these relatively coarse grids it is interesting that the approximation of the pdf is already a large improvement over the delta function of the global mean, and that the general shape of the pdf is recovered. Product mass fraction profiles obtained from using these pdfs in (11) have errors of the order of 20%.

Nevertheless there are clear differences between the true and the approximate pdfs. A sizable percentage of the pure fluid that should be associated to the delta functions at $\xi = 0$ and $\xi = 1$ has been aliased as mixed fluid into the central peak. This is especially evident deep into the layer (Fig. 2.a) where the unmixed regions are presumably of small size and are almost completely obliterated by the filter.

3.2 The Beta subgrid model

To improve the approximation in the previous section it was noted in (Cook & Riley 1994) that, if the subgrid variance (8) were known at each grid point, it should be possible to make a reasonable guess as to the form of the subgrid pdf, $p_h(\xi;\, \overline{\xi},\, \xi_h')$, and to obtain a better estimate of the true pdf in terms of the joint pdf of those two subgrid variables

$$\overline{p}(\xi) = \int p(\overline{\xi},\, \xi_h')p_h(\xi;\, \overline{\xi},\, \xi_h')\, \mathrm{d}\overline{\xi}\, \mathrm{d}\xi_h'. \tag{13}$$

In the particular model proposed in that paper, the subgrid pdf is represented as a Beta distribution, $p_h \sim \xi^{a-1}(1-\xi)^{b-1}$, and the two exponents a and b are computed at each point from the values of $\overline{\xi}$ and ξ_h'.

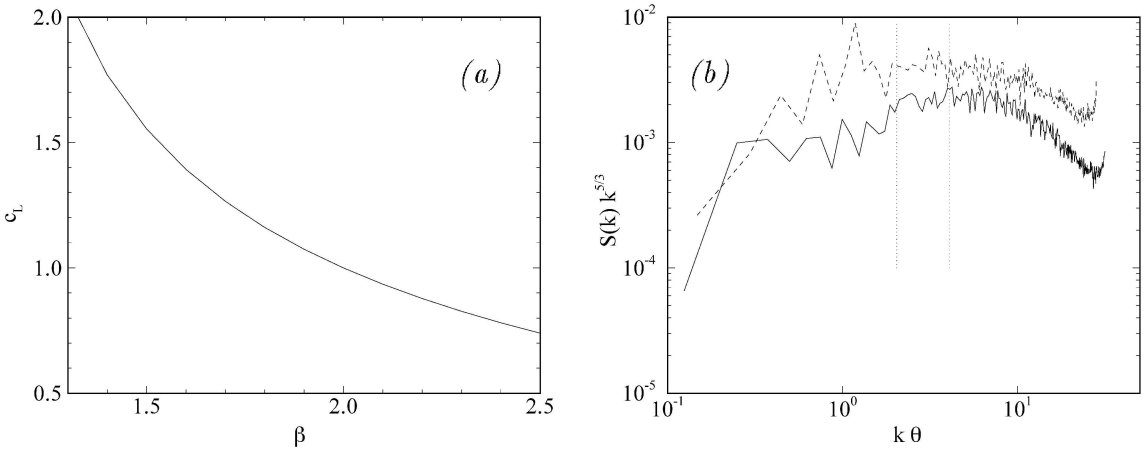

FIGURE 4. (a) Proportionality constant between band-passed and subgrid fluctuations, versus spectral slope. (b) Compensated scalar longitudinal spectra at the central planes (arbitrary units). ——— : unforced layer. ---- : forced. Vertical dotted lines are $kh = \pi$ for the two filters used in Fig. 3.b.

This correction needs the subgrid scalar variance, ξ_h', which is generally not given by the LES equations, but the same paper suggests that it may be obtained by a similarity argument from the behavior of the scalar at scales close to grid filter. Consider in our implementation two filter levels (Fig. 3.a). The first one is the grid filter of width h, which is represented by the dashed squares. The test filter $\widehat{\xi}$ is formed by averaging a 2^3 cubic box of contiguous, non-overlapping, grid values. In this implementation

$$\widehat{\overline{\xi}} = \widehat{\xi}, \tag{14}$$

and we can define the subgrid variance at the test level

$$\xi_{2h}'^2 = \widehat{\xi^2} - \widehat{\xi}^2. \tag{15}$$

Neither (15) nor (8) are known, but they can be combined to give a band-passed "Leonard" term which, using (14), can be written as

$$L^2 = \xi_{2h}'^2 - \widehat{\xi_h'^2} = \widehat{\overline{\xi}^2} - \widehat{\overline{\xi}}^2. \tag{16}$$

The right-hand side involves only filtered quantities, and can be computed as the standard deviation of $\overline{\xi}$ within the box defining the test filter. The similarity assumption is that

$$\xi_h' = c_L L, \tag{17}$$

and is seen to be reasonable in Fig. 3.b, where it is tested for the central part of the forced layer.

The proportionality constant can be estimated by assuming a form for the scalar spectrum, $S(k) \sim k^{-\beta}$. The subgrid variance is obtained by filtering the spectrum

through the transfer function of the filter, which has the form $F(kh)$. The result is that $\xi_h'^2 \sim h^{\beta-1}$ and, from (17)

$$c_L = (2^{\beta-1} - 1)^{-1/2}. \tag{18}$$

This quantity, which assumes an infinite Reynolds number in that it integrates the spectrum to $k \to \infty$, is plotted as a function of the spectral slope in Fig. 4.a. For the Kolmogorov slope $\beta = 5/3$ it has a value $c_L = 1.305$, which is the one used for the dashed line in Fig. 3.b, and represents the data well. In reality it is known that scalar spectra have slopes which are somewhat lower than 5/3 for Reynolds numbers in the range of our experiments (Sreenivasan 1996). This would imply proportionality constants somewhat higher than our value, but this effect is partly compensated by the presence of a Kolmogorov cutoff in the spectrum, which would lead to a lower value of c_L. Figure 4.b shows our scalar spectra and the position of our filters with respect to them. The fact that both effects compensate at our Reynolds number, and that they should vanish as $Re \to \infty$, suggests that the asymptotic value of c_L is a reasonable approximation for most of the Reynolds numbers of interest in LES.

In the two previous tests of the β-pdf model, the proportionality constant c_L was fitted to the data and found to be smaller than ours. Réveillon and Vervisch (1996) found $c_L = 0.5$ for a filter ratio of two, while Cook and Riley (1994) found $c_L \approx 1$ for $\hat{h}/\overline{h} = 1.8$, which would correspond to $\beta \approx 2.15$ according to (18), and to $c_L \approx 0.9$ for $\hat{h}/\overline{h} = 2$. Both simulations, however, were carried at Reynolds numbers substantially lower than ours. Réveillon and Vervisch worked at $Re_\lambda = 17$, for which there is no inertial range and no self-similar spectrum, and where turbulence is still barely developed. Cook and Riley do not give their Reynolds number, but their filters are only 6 times larger than the Batchelor scale, which would be near the right-most points in the spectra in Fig. 4, and within the dissipative range. Neither experiment can therefore be expected to agree with an inertial range prediction. It is probably a general rule that, if LES models are to behave independently of the type of flow, they should only be used in well-developed turbulence with filters in the inertial range.

The results of applying the β correction to the pdf in the previous section are shown in Fig. 5, where it is seen that error has decreased considerably with respect to Fig. 2 and, especially, that it is now relatively insensitive to the filter width. Note that the good behavior of the model is not only at the level of integral quantities, but at the detailed level of the pdf, implying that it should give good results for the average of *any* function of ξ and not only for the mass fraction (5). This includes the approximation of the pdf at a particular value of ξ, which is useful, for example, in evaluating source terms located at the flame. The figure includes the Beta distributions corresponding to the global averages and (true) standard deviations at each plane, as would be used in RANS.

Although they are not included in the figure, there is no appreciable difference between the LES results obtained using the true value of ξ_h' and those obtained using the estimation (17).

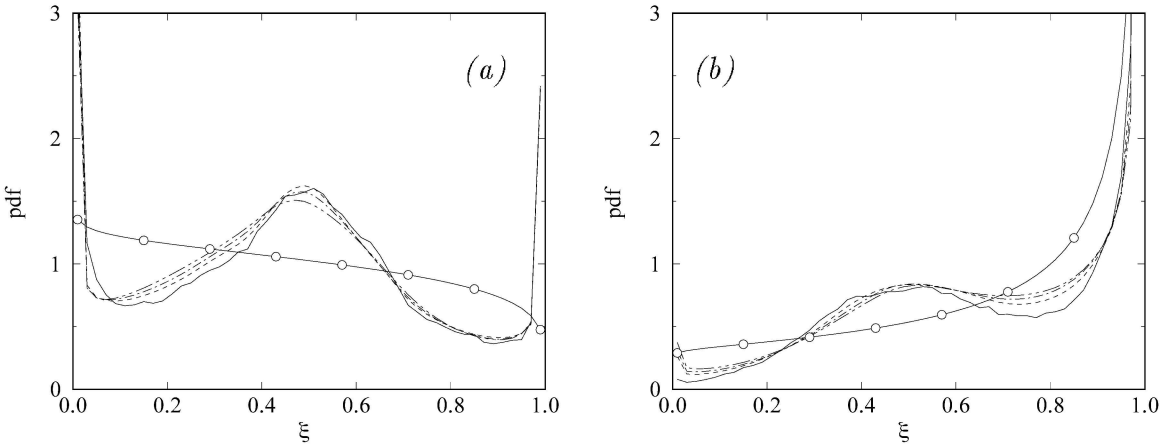

FIGURE 5. Mixture fraction pdfs from LES using the similarity β subgrid model. Forced layer. (a) $y/\theta = 0$. (b) $y/\theta = 3$. ——— : no filter. - - - - : $h/\theta = 0.55$. —·— : 0.77. —··— : 0.99. –o– : Beta distributions using the global mean and standard deviation for each plane.

It is curious that, when the RANS pdfs are used to compute the mean value of the mass fraction (5), the result is within a few percent of the actual one, but it is clear from Fig. 5 that this is due to compensating errors and that it cannot be extrapolated to other quantities.

3.3 Mean profiles

The results of using the approximate pdfs of the previous section to compute mean profiles of various quantities are presented in Fig. 6, in which the degree of difficulty increases from top to bottom and from the left to the right. Plots on the left of the page are computed for a stoichiometric mass fraction $\xi_s = 1/2$, for which the flame is roughly in the middle of the mixing layer. There the fluid is relatively well mixed, and the results should be comparable to those obtained in homogeneous turbulence. Those on the left of the page are for $\xi_s = 1/9$, which corresponds to global models of the H_2–O_2 reaction. For this stoichiometry the flame is near the edge of the mixing layer, in the interface between mixed and unmixed fluid, and LES may be expected to have more problems. The first two plots are mass fraction profiles obtained from the relatively smooth function (5). Those in the middle are profiles of Y_p^4, which is proportional to the fourth power of the temperature, and would therefore be a rough model for radiative heat in a flow with a real, hot, flame. This function (see Fig. 7.a) is much sharper than Y_p and is therefore sensitive to the local values of the pdf, in spite of which the errors in the mean profile are still small. The last two plots are the values of the pdf at a given ξ_s and are the most sensitive test of the three. They are also the ones for which the errors are larger, but it is remarkable that the general form of the profile is still captured and that the errors stay, at worse, of the order of 25%.

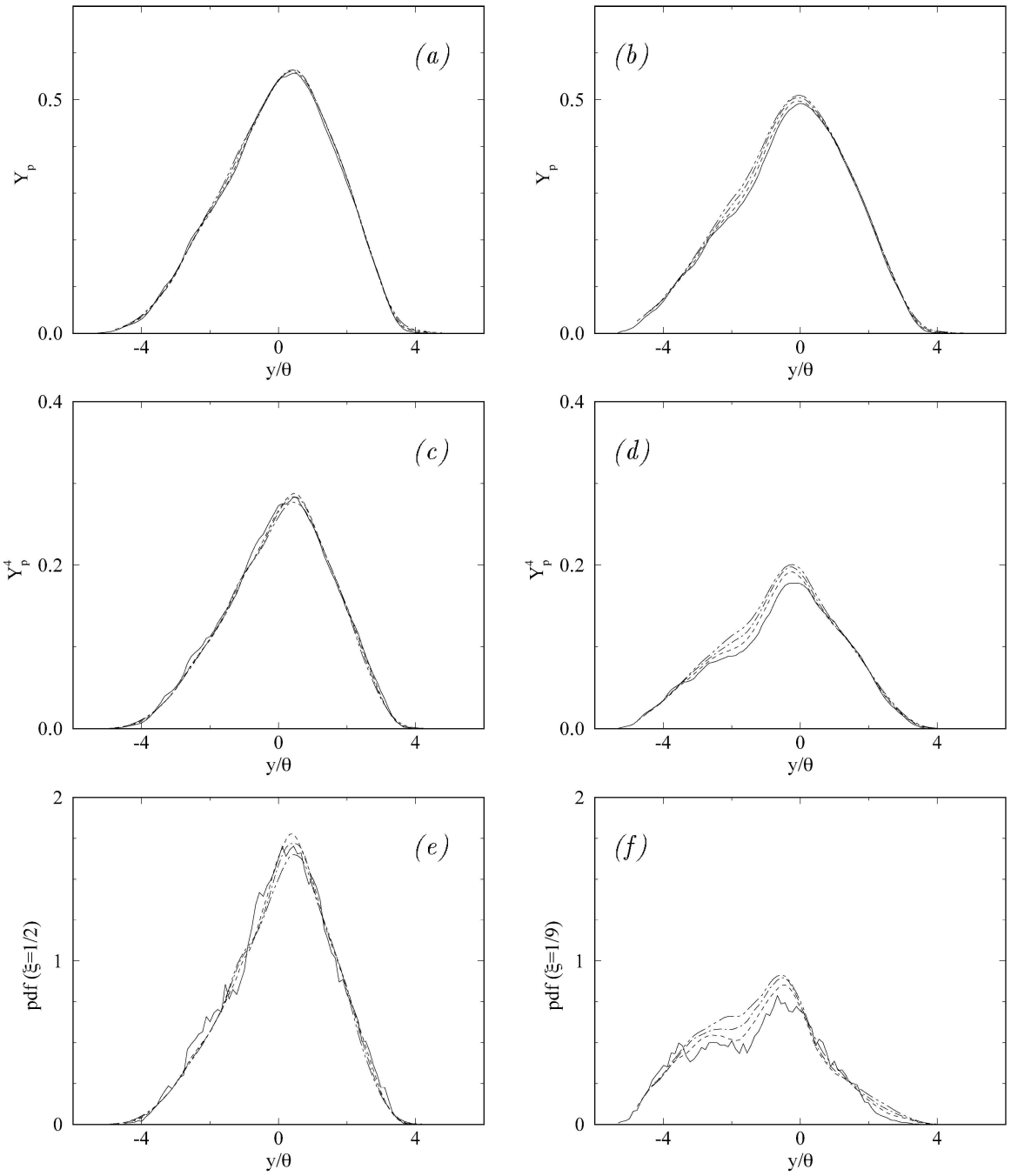

FIGURE 6. Average profiles for different functions in the forced layer. (a)–(b): Product mass fraction Y_p. (c)–(d): "Radiation" source Y_p^4. (e)–(f): Pdf(ξ_s). (a), (c) and (e) are for $\xi_s = 1/2$. The other three are for, $\xi_s = 1/9$.

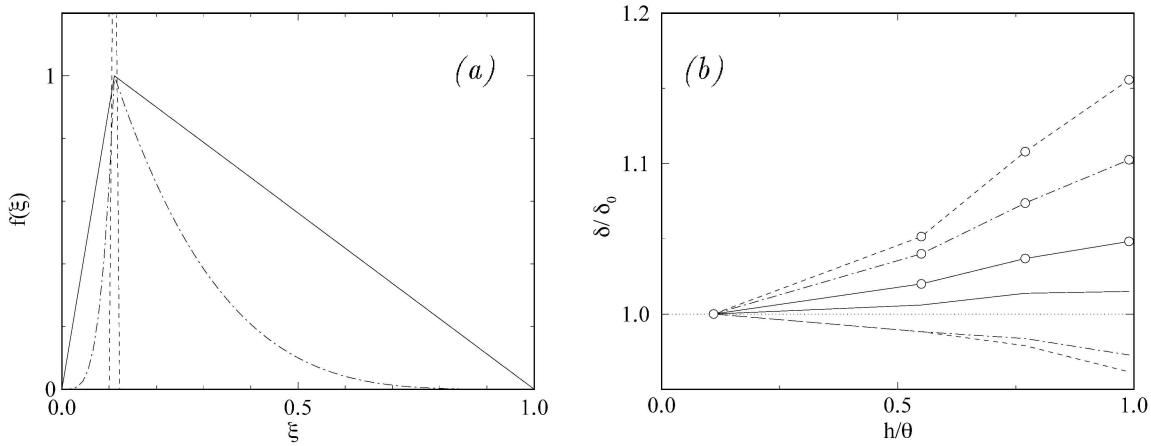

FIGURE 7. (a) The three functions used for the profiles in Fig. 6. $\xi_s = 1/9$. (b) Relative variation of the profile thickness with filter width. Forced layer. Lines with symbols are for $\xi_s = 1/9$. Other lines are for $\xi_s = 1/2$. ——— : Y_p. —·— : Y_p^4. ---- : Delta function with $\Delta\xi = 0.02$.

For any profile which vanishes at $y = \pm\infty$ we can define a "thickness"

$$\delta_f = \int_{-\infty}^{\infty} f(y)\,\mathrm{d}y, \tag{19}$$

which is proportional to the total amount of the particular quantity contained in the layer, and which can be used to quantify the global error of the approximation. Note that this thickness is unchanged by the filtering, $\delta_{\overline{f}} = \delta_f$. The results for the different profiles of Fig. 6 are presented in Fig. 7.b, where they have been normalized with their DNS values. The errors for $h/\theta < 1$ vary from better than 5% for the product mass fraction, to about 15% for the pdf. They are, as expected, generally larger for flames near the interface than for those at the center of the mixed region.

4. Finite rate effects

If the speed of the chemical reaction is large but not infinite, it is still possible to treat the combustion problem as a perturbation of the Burke-Schuman limit that we have used up to now. In this "flamelet" regime the deviations from infinitely fast chemistry are confined to a thin region around the location of the stoichiometric mixture fraction, whose width is a function of the Damköhler number.

Although the reaction zone is typically thin, there are cases in which the non-equilibrium effects are globally important. One such example is the H_2–O_2 reaction, in which an intermediate species is the H radical which, even in small amounts, controls the global exothermic properties. A simplified scheme

$$3\,\mathrm{H_2} + \mathrm{O_2} \rightarrow 2\,\mathrm{H_2O} + 2\,\mathrm{H}, \tag{20.a}$$

$$2\,\mathrm{H} + \mathrm{M} \rightarrow \mathrm{H_2} + \mathrm{M}, \tag{20.b}$$

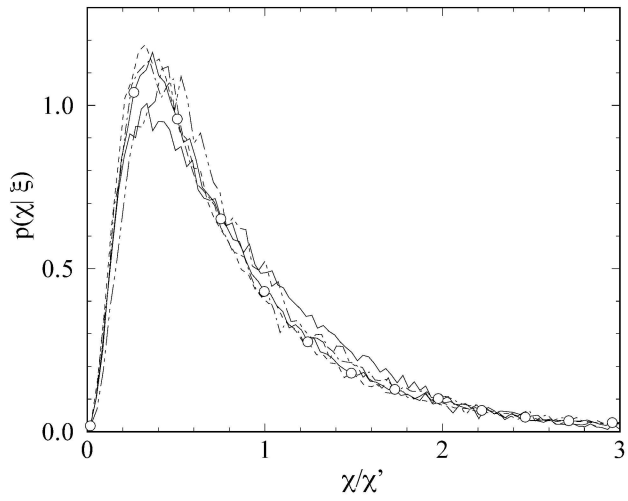

FIGURE 8. Pdfs of the mixture fraction gradients conditioned on the mixture fraction and compiled at different locations across the forced layer. ——— : $\xi = 0.2$. – – – – : 0.5. —·— : 0.8. —··— : 0.2. –○– : 0.5. The first three curves are for $y/\theta \in (-1, 1)$, $\langle\xi\rangle = 0.46$. The last two are for $y/\theta \in (1, 3)$, $\langle\xi\rangle = 0.72$.

was analyzed in (Sánchez *et al.* 1995). The first reaction is very fast and can be described by a conserved mixture fraction ξ and by an infinitely thin flame located at its stoichiometric isolevel ξ_s, while the second one is slower and leads to finite reaction rate corrections. The Damköhler number is defined as $D = (\kappa\chi^2 t_r)^{-1}$, where κ is the diffusion coefficient of the scalars, $\chi = \nabla\xi$ is the mixture fraction gradient at the stoichiometric level, and t_r is a chemical time which is only a weak function of temperature. The combination $\kappa\chi^2$ is usually called the scalar dissipation. In our approximation the only variable is χ, which therefore controls the structure of the flame. Other reactions involving radicals are technologically important. For example, the NO_x production in air is controlled by the temperature and by the concentration of the O radical.

It turns out that both the thickness and the maximum concentration in the radical containing region are proportional to $D^{-1/3}$, so that the total mass of H radical per unit flame area is proportional to

$$m \sim D^{-2/3} \sim \kappa^{2/3}\chi^{4/3}. \tag{21}$$

There is a chemical energy associated to this mass which leads to a lowering of the flame temperature. The dependence on a power of the gradients is common in many other examples of slightly out-of-equilibrium reactions (Williams 1985), although the exponents change from one case to another. Assume in general that $m = \kappa^\alpha \chi^{2\alpha}$. We can estimate the average mass fraction of radical by a procedure similar to that used to derive (6). If S is the area per unit volume we write

$$\langle Y_H \rangle = \int_S m \, \mathrm{d}S, \tag{22}$$

which we wish to transform into a probability integral. Introduce the joint pdf of χ and ξ and define $\mathrm{d}n$ as the element of length normal to the flame, located at $\xi = \xi_s$. We can define the volume element both in terms of the geometry and of the pdf

$$\mathrm{d}V = \mathrm{d}n\,\mathrm{d}S = p_2(\chi,\,\xi)\,\mathrm{d}\chi\,\mathrm{d}\xi, \tag{23}$$

from where, using that $\chi = \mathrm{d}\xi/\mathrm{d}n$, it follows that $\mathrm{d}S = \chi\, p(\chi,\,\xi)\,\mathrm{d}\chi$, and

$$\langle Y_H \rangle = \int_{\xi=\xi_s} \chi\, m(\chi) p_2(\chi,\,\xi)\,\mathrm{d}\chi = p(\xi_s) \int_0^\infty \chi\, m(\chi) p(\chi|\,\xi_s)\,\mathrm{d}\chi. \tag{24}$$

The new pdf which appears in the second part of this equation is the pdf of gradients *conditioned* to $\xi = \xi_s$. Note that (24) has the same form as (6) for a function

$$f(\xi) = C_\chi \delta(\xi - \xi_s), \qquad C_\chi = \int_0^\infty \chi\, m(\chi) p(\chi|\,\xi_s)\,\mathrm{d}\chi, \tag{25}$$

which is a delta function at the location of the flame, with a prefactor which depends on a moment of the conditional gradient pdf.

Formulas of this type have been known for a long time in the context of nonequilibrium chemistry (Bilger 1976), and the joint pdf of the gradients and of a mixing scalar has been the subject of intensive study. There is general consensus that the *unconditional* gradient pdf is approximately log-normal (Kerstein & Ashurst 1984, Anselmet & Antonia 1985, Eswaran & Pope 1987, Pumir 1994, Holzer & Siggia 1994), a form for which there is incomplete theoretical support (Gurvich & Yaglom 1967, Meyers & O'Brien 1981) but which seems to be only an approximation to the real one. There is less consensus on the conditional pdf and, in particular, on whether the conditional variance of the gradients is correlated to the value of ξ_s or to the local turbulent dissipation ϵ.

We have checked conditional gradient pdfs for our two shear layers and the results are shown in Figs. 8 to 10. It is seen in the first figure that the form of the pdf is fairly independent of both ξ_s and of the location in the flow, when each pdf is referred to its own standard deviation χ'. It also has a general log-normal shape, but is not really log-normal. Note that the figure includes pdfs conditioned on values of ξ_s close to zero, but compiled at locations at which the mean value of ξ is close to one.

Figure 9 presents a two-dimensional map of the conditional $\chi'(\xi)$, as a function of ξ and of the location across the layer. It was found that the map was more uniform if the conditional χ' was normalized with χ'_0, the unconditional standard deviation at the center of the layer, than when the normalization was done with the unconditional χ' at the particular y location. The first choice is used in the figure. It is seen that the dissipation has a central plateau, in which $\chi'/\chi'_0 \approx 1$, but becomes larger near the edges of the layer, and vanishes at $\xi = 0$ and $\xi = 1$. The latter is an obvious property of laminar unmixed fluid and will be discussed below. The decline is, on the other hand, quite local and only happens when ξ is

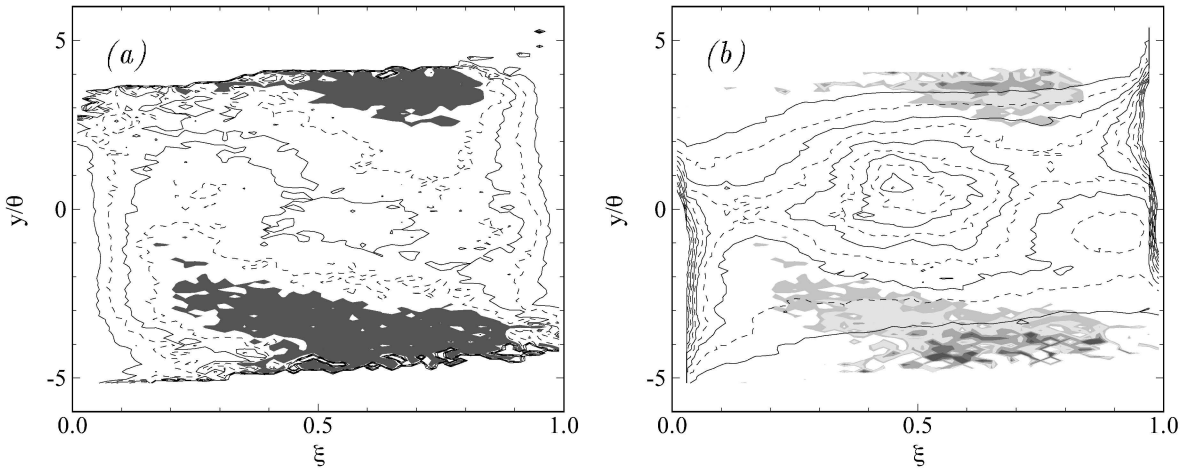

FIGURE 9. (a) Standard deviation of the scalar gradient magnitude as a function of y/θ, conditioned on ξ and normalized with the unconditional χ_0' at the central plane. Isolines are $\chi'/\chi_0' = 0.6\,(0.2)\,1.2$, and shaded area is $\chi'/\chi_0' \geq 1.4$. Forced layer. (b) Pdf of ξ for the same flow. Each horizontal section represents the pdf over one plane. Isolines $p(\xi) = 0.1\,(0.2)\,2.1$. Isolines alternate line style for clarity, and shaded regions correspond in both figures.

within 10% of the unmixed fluid. It should therefore not be important unless the stoichiometric ξ_s is very close to 0 or 1. The rise near the edges of the layer is real, but it corresponds to combinations of mixture fraction and location which are relatively improbable, as can be seen in Fig. 9.b, in which the areas of high scalar dissipation have been overlaid on a two dimensional map of the mixture fraction pdf. It is clear that they correspond to events whose probability is mostly below 10% and which will not have a large weight in (24).

In Fig. 10 we have presented cross-stream profiles of $\chi'(\xi)/\chi_0'$ for various values of ξ. These are essentially vertical cross-sections of Fig. 9.a, but they have been included to give some quantitative information on the magnitude of the deviations of the scalar dissipation from its unconditional value, and to present data from the unforced layer. As in the previous figure it is seen that the scalar dissipation in the central part of the layer, where the fluid is well mixed, is more or less constant and equal to its unconditioned maximum value, but that the gradients conditioned on mixtures fractions close to the free stream values and all the gradients near the edges of the layer have standard deviations that may differ from the global maximum by almost a factor of two. They also have a characteristic parabolic shape. Most of these high deviations occur at places at which the absolute probability of ξ is small, as seen on the figures on the right hand side of 10, which are conditioned on $p(\xi) > 0.1$, and they will only have a small effect on (24), but the effect is real and begs, at least, for some theoretical explanation.

It is also interesting to note that the general magnitude of the gradients is low. The value of $\chi_0'\theta$ is 1.5 for the unforced case and 2.0 for the forced one, so that the peak of the distributions in Fig. 8 is for gradients of the order of those of the

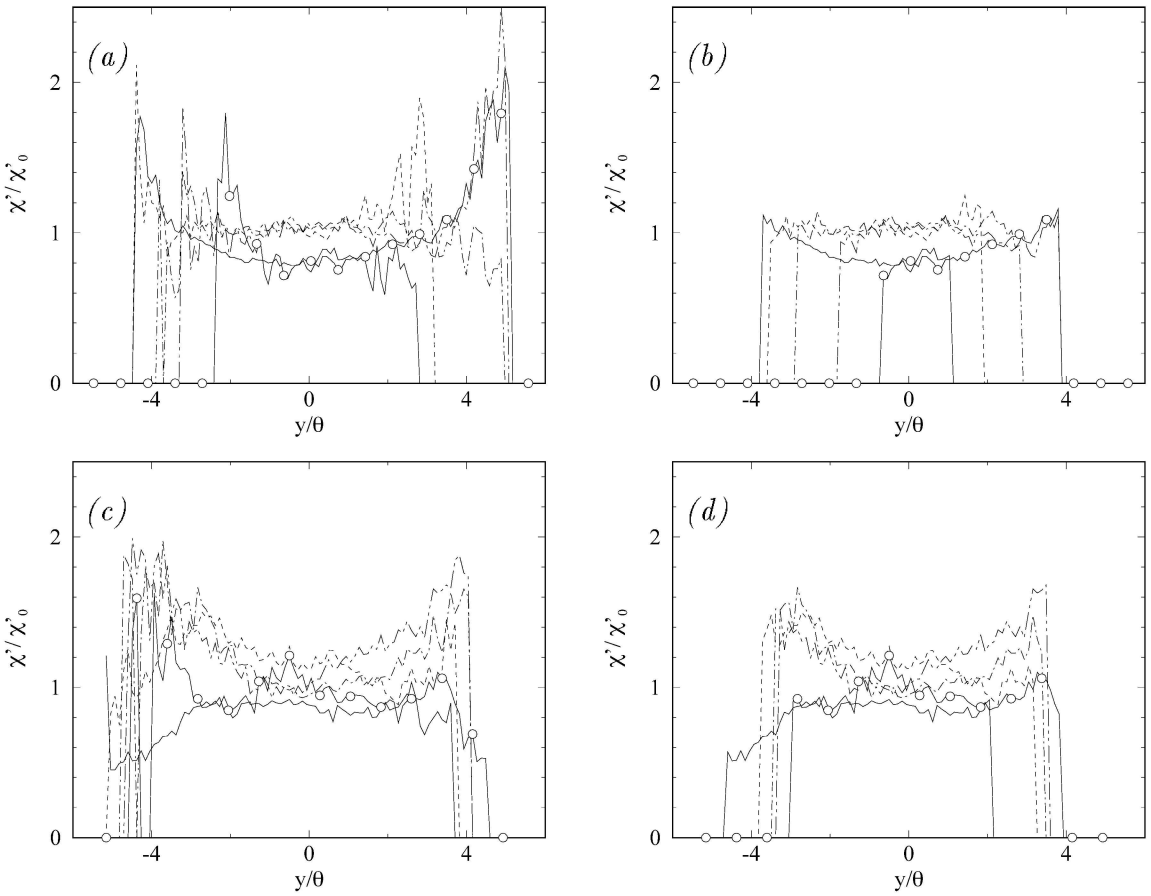

FIGURE 10. Variation of the conditional standard deviation of the gradients across the layer, as a function of ξ. ——— : ξ=0.1. ---- : 0.3, —·— : 0.5. —··— : 0.7. –o–: 0.9. (a) and (b) are for the unforced layer; (c) and (d) for the forced one. (a) and (c) present full profiles, but (b) and (d) are only for those points in which $p(\xi) > 0.1$.

mean ξ profile. Since high gradients lower the Damköhler number and may lead to extinction of the flame, the probability of local extinction for a given flow can be read from these distributions.

In LES computations it might be harder to estimate the value of χ_0' than that of the subgrid scalar fluctuation. The problem is that while the spectrum of ξ decreases with wavenumber approximately like $S(k) \sim k^{-5/3}$, that for the gradient increases as $k^2 S(k) \sim k^{1/3}$. Thus, while most of the contribution to ξ' comes from the resolved large scales, χ' comes mostly from the unresolved small ones. In terms of the standard LES or modeling equations, ξ'^2 is equivalent to the subgrid energy, while χ'^2 is equivalent to the subgrid dissipation. Conservation equations and closures for the subgrid dissipation have been written among others by Newman, Launder & Lumley (1981) and Elgobashi & Launder (1983).

The "engineering" consequences of the errors due to the gradient pdfs are summarized in Fig. 11. Assume that we are interested in computing the total amount of

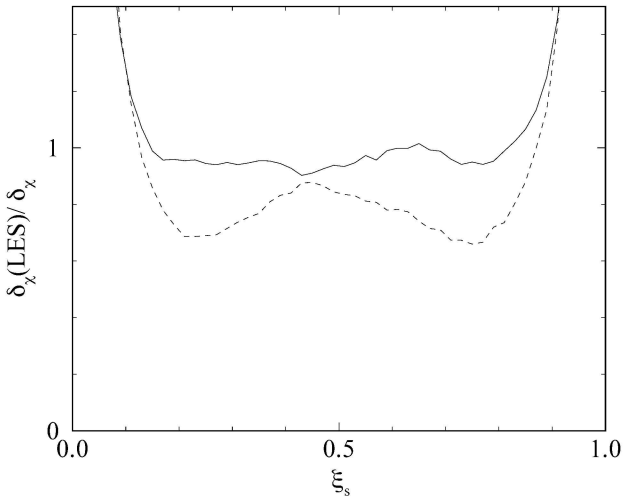

FIGURE 11. Computed scalar dissipation thickness as defined in text, compared to its DNS value. $h/\theta \approx 0.9$. ——— : unforced layer. ---- : forced.

H radical in the example (20), and that we use as a subgrid model for the gradients an average pdf taken from Fig. 8, and a representative unconditional χ_0' estimated for the center of the layer. Using (24) and integrating as in (19), we obtain a "radical" thickness which is the integral across the layer of the $\alpha + 1$ moment of the conditional pdf of the gradients, weighted with the pdf of the stoichiometric mixture fraction. This can be compared with the result of using the true distributions, and gives a global error due to the simplified assumption on the gradients. The result depends on the exponent α, but it is especially simple in the case of $\alpha = 1$ since the $\alpha + 1$ moment is then proportional to the scalar dissipation, and the integral can be obtained directly from the data in Fig. 9. In this case the approximation is equivalent to taking everywhere χ_0' as an approximation to $\chi'(\xi_s)$. This normalized thickness is not very different from the results for $\alpha = 4/3$, and is presented in Fig. 11. It is seen that, because the deviations from a universal distribution are mostly associated with places in which $p(\xi_s)$ is small, the final errors are still reasonable, especially for the unforced case, although they become $O(1)$ when the stoichimetric ratio approaches 0 or 1.

The reason for this failure is clearly that we have not taken into account that gradients have to vanish when the scalar is very near its maximum or minimum value. Simple engineering models should be able to alleviate this problem, but they are beyond the purpose of this paper. It is, however, interesting to estimate the width of the region for which a correction needs to be applied, which either from Fig. 9 or 11 is in this case about $\Delta\xi \approx 0.1$, but which can be related to the Reynolds number of the simulation. It follows from the form of the scalar spectrum that, for $Sc = O(1)$, most of χ' is associated with scales of the order of the Kolmogorov length η, and that the scalar fluctuations at length ℓ are $\Delta\xi_\ell \approx \xi'(\ell/L_\epsilon)^{1/3}$, where

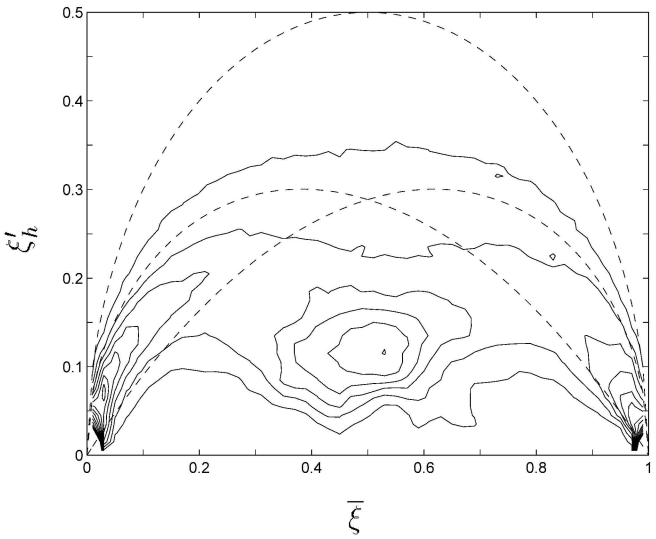

FIGURE 12. Joint pdf for $\overline{\xi}$ and the subgrid fluctuation ξ_h'. Forced layer. $h/\theta = 0.88$. $y/\theta \in (-2, 2)$. Isolines are $p_2(\overline{\xi}, \xi_h') = 1(2)21$. Dashed semicircle is the limit of possible $(\overline{\xi}, \xi_h')$ combinations. Lower dashed lines are the limits below which the Beta distribution looks like a single broadened spike.

L_ϵ is an integral length. Since $L_\epsilon/\eta \approx Re_\lambda^{3/2}$ (Tennekes & Lumley 1972), it follows that the scalar fluctuations which carry the gradients are of order

$$\Delta\xi \approx \xi' Re_\lambda^{-1/2}, \tag{26}$$

which in our case 0.03. As long as ξ_s and $1 - \xi_s$ remain large with respect to this value, the small eddies should not be affected by the proximity to the level of the unmixed fluid, but if they are of the same order as (26), large gradients become impossible. This suggests that the width of the lateral bands in Fig. 11 should decrease as the Reynolds number increases, but it would be interesting to get experimental confirmation of that estimate.

5. Conclusions

We have shown that relatively simple subgrid models for the pdf of a conserved scalar can be used to obtain useful engineering approximations to global quantities in LES simulations of reacting nonpremixed turbulent shear flows in the fast chemistry limit. This is true even when the flow, in our case two different mixing layers, contains substantial intermittency.

The magnitude of the approximation error varies from less than 5% for the total amount of generated products, to about 15% for the pdf of the scalar itself. When finite reaction rate corrections are introduced in the flamelet limit, the model has to be extended to the pdf of the scalar gradients, conditioned on the value of the scalar. We have shown that those pdfs have an approximately universal form and that they can be expressed in terms of a single parameter, the conditional scalar

dissipation, which varies little except at places in which the probability of finding mixed fluid is low. It is possible in those cases to obtain the global concentration of intermediate products (e.g. radicals) with errors which stay in the 20-30% range, except for reactions with stoichiometric mixture fractions very near those of the free streams. We have argued that the range of stoichiometric ratios for which the approximation fails should decrease with increasing Reynolds numbers. It should be clear, however, that even within this range the integrated quantities such as product concentration or radiation thickness are well predicted (Fig. 7).

The particular approximation used in our experiments is the β model of (Cook & Riley 1994), but it is clear from the lack of correspondence between actual and assumed pdfs that other models might work as well. This also follows from similar observations of Cook & Riley in their paper, and is in contrast with the situation in RANS, in which it is known that good subgrid models have to be used for the assumed pdf if any but the simplest quantities are to be computed accurately (Fig. 5). It is important to understand the reason for this difference, which is essentially contained in Fig. 2, where the scalar pdfs are reasonably well approximated even in the absence of a subgrid model. This means that most of the scalar fluctuations are associated to scales which are resolved by the LES, even for coarse grids like the ones used here. All that is left for the model is to correct situations in which the subgrid fluctuation is strong enough that the use of the average as a representation of the pdf is no longer appropriate.

The situation would still be hopeless if those fluctuations were large enough to allow for a considerable latitude in the choice of subgrid pdfs, but this is fortunately not the case. Consider the $(\overline{\xi}, \xi_h')$ plane in Fig. 12. It can be shown that there can be no points above the dashed semicircle, and that pdfs that fall on the semicircle must be formed exclusively by unmixed fluid with $\xi = 0$ and $\xi = 1$. In the same way, pdfs on the horizontal axis are single delta functions of uniform fluid with $\xi = \overline{\xi}$. Pdfs near that axis are roughly spread deltas, and those near the semicircle, spread bimodals. The border between the two cases varies for different models, but it is always near the two intermediate dashed lines in the figure, which correspond to the β-model. Below those lines, the pdf are bells, and almost any model should be equivalent. Pdfs within the two crescents correspond to spread deltas near one or the other free stream, and are also easy to model. Pdfs in the high-fluctuation central part of the diagram are harder, and are likely to depend on more than two parameters.

We have overlaid on the diagram a typical joint pdf for $\overline{\xi}$ and ξ_h', for a relatively wide filter in the intermittent "hard" flow but, even in this case, most of the mass of the distribution is associated with pdfs within the easily modeled part of the diagram. The Beta distributions form a flexible set of pdfs which interpolate smoothly between the different cases, and they provide a simple numerical tool to evaluate the necessary integrals. This explains their practical success, but the reason why the approximation works lies in the small value of the subgrid standard deviations in Fig. 12. Since we have seen in Fig. 3 that these deviations can be estimated from large-scale quantities using an infinite Reynolds assumption on the upper limit of

the spectrum, it is unlikely that much higher values might be found in other flows.

The small values of the fluctuations are also the reason why our relatively crude estimation of ξ_h' works so well. Even large errors in this estimation have relatively small effects on the final results, and some experiments in which the estimated subgrid fluctuations where systematically increased or decreased by 20% did not show any appreciable differences with the results shown here.

The convergence of the gradients also needs some discussion. It appears at first sight that, since the dominant contribution to χ'^2 comes from the high end of the spectrum, the estimates for this quantity would depend of the value of the Batchelor scale, and would diverge at high Reynolds numbers. What is needed in (21), however, is not χ'^2 but the scalar dissipation $\kappa\chi'^2$, and it is easy to see that, for a $k^{-5/3}$ spectrum, this quantity is independent of Reynolds number.

REFERENCES

Anselmet, F. & Antonia, R. A. 1985 Joint statistics between temperature and its dissipation in a turbulent jet. *Phys. Fluids.* **28,** 1048-1054.

Bilger, R. W. 1976 The structure of diffusion flames. *Combust. Sci. Tech.* **13,** 155-170.

Bilger, R. W. 1989 Turbulent diffusion flames. *Ann. Rev. Fluid Mech.* **21,** 101-135.

Breidenthal, R. E. 1981 Structure in chemically mixing layers and wakes using a chemical reaction. *J. Fluid Mech.* **109,** 1-24

Broadwell, J. E. & Breidenthal,R.E. 1982 A simple model of mixing and chemical reaction in a turbulent shear flow. *J. Fluid Mech.* **125,** 397-410.

Cook, A. W. & Riley, J. J. 1994 A subgrid model for equilibrium chemistry in turbulent flows. *Phys. Fluids.* **6,** 2868-2870.

Dopazo, C. 1977 On conditional averages for intermittent turbulent flows. *J. Fluid Mech.* **81,** 433-438.

Elgobashi, S. E. & Launder, B. E. 1983 Turbulent time scales and the dissipation rate of temperature variance in the thermal mixing layer. *Phys. Fluids.* **26,** 2415-2419.

Eswaran, V. & Pope, S. B. 1988 Direct numerical simulations of the turbulent mixing of a passive scalar. *Phys. Fluids.* **31,** 506-520.

Gurvich, A. S. & Yaglom, A. M. 1967 Breakdown of eddies and probability distributions for small-scale turbulence, boundary layers and turbulence. *Phys. Fluids Suppl.* **10,** S 59-65.

Holzer, M. & Siggia, E. D. 1994 Turbulent mixing of a passive scalar. *Phys. Fluids.* **6,** 1820-1837.

Kerstein, A. R. & Ashurst, W. T. 1984 Lognormality of gradients of diffusive scalars in homogeneous, two-dimensional mixing systems. *Phys. Fluids.* **27,** 2819-2827.

KOLLMAN, W. 1984 Prediction of intermittency factors for turbulent shear flows. *AIAA J.* **22,** 486-492.

KOLLMAN, W. & JANICKA, J. 1982 The probability density function of a passive scalar in turbulent shear flows. *Phys. Fluids.* **25,** 1755-1769.

KONRAD, J. H 1976 An experimental investigation of mixing in two-dimensional turbulent shear flows with applications to diffusion-limited chemical reactions. *PhD thesis.* Caltech (CIT-8-PU).

KOOCHESFAHANI, M. M. & DIMOTAKIS, P. E. 1986 Mixing and chemical reactions in a turbulent liquid mixing layer. *J. Fluid Mech.* **170,** 83-112.

LARUE, J C. & LIBBY, P. A. 1974 Temperature fluctuations in the plane turbulent wake. *Phys. Fluids.* **17,** 1956-1967.

LESIEUR, M. & ROGALLO, R. S. 1989 Large-eddy simulation of passive scalar diffusion in isotropic turbulence. *Phys. Fluids.* **A 1,** 718-722.

LIBBY, P. A. 1975 On the prediction of intermittent turbulent flows. *J. Fluid Mech.* **68,** 273-295.

LIBBY, P. A. & WILLIAMS, F. A. (editors) 1994 Turbulent reacting flow, Academic Press.

LIN, C. H. & O'BRIEN, E. E. 1974 Turbulent shear flow mixing and rapid chemical reaction: an analogy. *J. Fluid Mech.* **64,** 195-206.

MEYERS, R. E. & O'BRIEN, E. E. 1981 The joint pdf of a scalar and its gradient at a point in a turbulent fluid. *Combust. Sci. Tech.* **26,** 123-134.

MOIN, P., SQUIRES, K., CABOT, W. & LEE, S. 1991 A dynamic subgrid-scale model for compressible turbulence and scalar transport. *Phys. Fluids.* **3,** 2746-2757.

MUNGAL, M. G. & DIMOTAKIS, P. E. 1984 Mixing and combustion with low heat release in a turbulent shear layer. *J. Fluid Mech.* **148,** 349-382.

NEWMAN, G. R., LAUNDER, B. E. & LUMLEY, J. L. 1981 Modeling the behavior of homogeneous scalar turbulence. *J. Fluid Mech.* **111,** 217-232.

POPE, S. B. 1985 PDF methods for turbulent reacting flows. *Prog. Energy Combust. Sci.* **11,** 119-192.

POPE, S. B. & CORREA, S. M. 1988 Joint pdf calculation of a non-equilibrium turbulent diffusion flame. *21st. Symp. (Int.) Combust.,* 1341-1348. Pittsburg. Combust. Inst.

PUMIR, A. 1994 A numerical study of the mixing of a passive scalar in three dimensions in the presence of a mean gradient. *Phys. Fluids.* **6,** 2118-2132.

RÉVEILLON, J. & VERVISCH, L. 1996 Dynamic large eddy simulation and subgrid pdf for nonpremixed turbulent flame modeling. *Preprint.*

ROGERS, M. M. & MOSER, R. D. 1994 Direct simulation of a self-similar turbulent mixing layer. *Phys. Fluids.* **6,** 903-923.

Sánchez, A. L., Liñán, A., Williams, F. A. & Balakrishnan, G. 1995 *Combust. Sci. Tech.* **110,** 277-301.

Sreenivasan, K. R. 1996 The passive scalar spectrum and the Obukhov-Corrsin constant. *Phys. Fluids.* **6,** 189-196.

Tennekes, H. & Lumley, J. L. 1972 *A first course in turbulence.* MIT Press.

Williams, F. A. 1985 *Combustion Theory*, 2nd. ed., Benjamin-Cummings. Menlo Park, Ca.